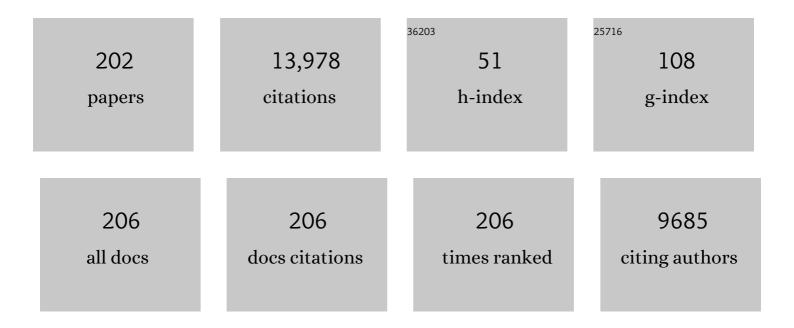
List of Publications by Year in descending order

Source: https://exaly.com/author-pdf/9513739/publications.pdf Version: 2024-02-01



SINA FADSILI

#	Article	IF	CITATIONS
1	Deep learning-based classification and segmentation of retinal cavitations on optical coherence tomography images of macular telangiectasia type 2. British Journal of Ophthalmology, 2022, 106, 396-402.	2.1	8
2	BiconNet: An edge-preserved connectivity-based approach for salient object detection. Pattern Recognition, 2022, 121, 108231.	5.1	22
3	Open-source deep learning-based automatic segmentation of mouse Schlemm's canal in optical coherence tomography images. Experimental Eye Research, 2022, 214, 108844.	1.2	6
4	Editorial from the New Editor-in-Chief and the New Deputy Editor. Biomedical Optics Express, 2022, 13, 980.	1.5	0
5	Identifying Latent Stochastic Differential Equations. IEEE Transactions on Signal Processing, 2022, 70, 89-104.	3.2	4
6	VALIDATION OF A DEEP LEARNING-BASED ALGORITHM FOR SEGMENTATION OF THE ELLIPSOID ZONE ON OPTICAL COHERENCE TOMOGRAPHY IMAGES OF AN USH2A-RELATED RETINAL DEGENERATION CLINICAL TRIAL. Retina, 2022, 42, 1347-1355.	1.0	5
7	Machine Learning OCT Predictors of Progression from Intermediate Age-Related Macular Degeneration to Geographic Atrophy and Vision Loss. Ophthalmology Science, 2022, 2, 100160.	1.0	6
8	Integrated Visualization Highlighting Retinal Changes in Retinopathy of Prematurity From 3-Dimensional Optical Coherence Tomography Data. JAMA Ophthalmology, 2022, 140, 725.	1.4	3
9	Fast and accurate neuron segmentation and unmixing based on shallow U-Net. , 2022, , .		0
10	Open-Source Automatic Segmentation of Ocular Structures and Biomarkers of Microbial Keratitis on Slit-Lamp Photography Images Using Deep Learning. IEEE Journal of Biomedical and Health Informatics, 2021, 25, 88-99.	3.9	17
11	Retinal cavitations in macular telangiectasia type 2 (MacTel): longitudinal structure–function correlations. British Journal of Ophthalmology, 2021, 105, 109-112.	2.1	11
12	Lightweight Learning-Based Automatic Segmentation of Subretinal Blebs on Microscope-Integrated Optical Coherence Tomography Images. American Journal of Ophthalmology, 2021, 221, 154-168.	1.7	6
13	Intraoperative Retinal Changes May Predict Surgical Outcomes After Epiretinal Membrane Peeling. Translational Vision Science and Technology, 2021, 10, 36.	1.1	2
14	Anti-fibrotic activity of a rho-kinase inhibitor restores outflow function and intraocular pressure homeostasis. ELife, 2021, 10, .	2.8	32
15	57084 Combining artificial intelligence and robotics: a novel fully automated optical coherence tomography-based approach for eye disease screening. Journal of Clinical and Translational Science, 2021, 5, 122-122.	0.3	0
16	Weakly supervised individual ganglion cell segmentation from adaptive optics OCT images for glaucomatous damage assessment. Optica, 2021, 8, 642.	4.8	19
17	Unified k-space theory of optical coherence tomography. Advances in Optics and Photonics, 2021, 13, 462.	12.1	15
18	Local Anatomic Precursors to New-Onset Geographic Atrophy in Age-Related Macular Degeneration as Defined on OCT. Ophthalmology Retina, 2021, 5, 396-408.	1.2	8

#	Article	IF	CITATIONS
19	Segmentation of neurons from fluorescence calcium recordings beyond real time. Nature Machine Intelligence, 2021, 3, 590-600.	8.3	27
20	Microscope-Integrated OCT-Guided Volumetric Measurements of Subretinal Blebs Created by a Suprachoroidal Approach. Translational Vision Science and Technology, 2021, 10, 24.	1.1	3
21	COMPARISON OF SINGLE DRUSEN SIZE ON COLOR FUNDUS PHOTOGRAPHY AND SPECTRAL-DOMAIN OPTICAL COHERENCE TOMOGRAPHY. Retina, 2021, 41, 1715-1722.	1.0	9
22	Connectivity-based deep learning approach for segmentation of the epithelium in in vivo human esophageal OCT images. Biomedical Optics Express, 2021, 12, 6326.	1.5	11
23	Open-Source Automatic Biomarker Measurement on Slit-Lamp Photography to Estimate Visual Acuity in Microbial Keratitis. Translational Vision Science and Technology, 2021, 10, 2.	1.1	3
24	Mesoscopic photogrammetry with an unstabilized phone camera. , 2021, , .		4
25	Incoherent 3D k-space synthesis with volumetric optical coherence refraction tomography. , 2021, , .		1
26	Beyond Performance Metrics. Ophthalmology, 2020, 127, 793-801.	2.5	27
27	Quantitative Fundus Autofluorescence in Rhesus Macaques in Aging and Age-Related Drusen. , 2020, 61, 16.		7
28	Treated PDR Reveals Age-Appropriate Vision Deterioration But Distorted Retinal Organization. Translational Vision Science and Technology, 2020, 9, 3.	1.1	2
29	Integral role for lysyl oxidaseâ€likeâ€1 in conventional outflow tissue function and behavior. FASEB Journal, 2020, 34, 10762-10777.	0.2	20
30	Generative adversarial networks to predict treatment response for neovascular age-related macular degeneration: interesting, but is it useful?. British Journal of Ophthalmology, 2020, 104, 1629-1630.	2.1	6
31	Measurement Reliability for Keratitis Morphology. Cornea, 2020, 39, 1503-1509.	0.9	4
32	Learning Partial Differential Equations From Data Using Neural Networks. , 2020, , .		6
33	MimickNet, Mimicking Clinical Image Post- Processing Under Black-Box Constraints. IEEE Transactions on Medical Imaging, 2020, 39, 2277-2286.	5.4	22
34	Multimodal Coherent Imaging of Retinal Biomarkers of Alzheimer's Disease in a Mouse Model. Scientific Reports, 2020, 10, 7912.	1.6	16
35	Assessing Ganglion Cell Layer Topography in Human Albinism Using Optical Coherence Tomography. , 2020, 61, 36.		15
36	Long-term Evolution and Remodeling of Soft Drusen in Rhesus Macaques. , 2020, 61, 32.		27

#	Article	IF	CITATIONS
37	Baseline Visual Field Findings in the RUSH2A Study: Associated Factors and Correlation With Other Measures of Disease Severity. American Journal of Ophthalmology, 2020, 219, 87-100.	1.7	22
38	Deep learning-based single-shot prediction of differential effects of anti-VEGF treatment in patients with diabetic macular edema. Biomedical Optics Express, 2020, 11, 1139.	1.5	53
39	Spectroscopic optical coherence refraction tomography. Optics Letters, 2020, 45, 2091.	1.7	9
40	Multimodal handheld adaptive optics scanning laser ophthalmoscope. Optics Letters, 2020, 45, 4940.	1.7	6
41	Resolution enhancement and speckle reduction in coherence imaging: a k-space model of optical coherence refraction tomography (OCRT). , 2020, , .		0
42	Fully automatic quantification of individual ganglion cells from AO-OCT volumes via weakly supervised learning. , 2020, , .		1
43	Wavefront sensorless multimodal handheld adaptive optics scanning laser ophthalmoscope for in vivo imaging of human retinal cones. , 2020, , .		0
44	Demonstration of anatomical development of the human macula within the first 5Âyears of life using handheld OCT. International Ophthalmology, 2019, 39, 1533-1542.	0.6	9
45	Ocular amyloid imaging at the crossroad of Alzheimer's disease and age-related macular degeneration: implications for diagnosis and therapy. Journal of Neurology, 2019, 266, 1566-1577.	1.8	23
46	Optical coherence refraction tomography. Nature Photonics, 2019, 13, 794-802.	15.6	50
47	Computational modeling of retinal hypoxia and photoreceptor degeneration in patients with age-related macular degeneration. PLoS ONE, 2019, 14, e0216215.	1.1	22
48	Distribution of OCT Features within Areas of Macular Atrophy or Scar after 2 Years of Anti-VEGF Treatment for Neovascular AMD in CATT. Ophthalmology Retina, 2019, 3, 316-325.	1.2	17
49	Vascular Response to Sildenafil Citrate in Aging and Age-Related Macular Degeneration. Scientific Reports, 2019, 9, 5049.	1.6	20
50	Super-resolution retinal imaging using optically reassigned scanning laser ophthalmoscopy. Nature Photonics, 2019, 13, 257-262.	15.6	20
51	Estimation of Gestational Age via Image Analysis of Anterior Lens Capsule Vascularity in Preterm Infants: A Pilot Study. Frontiers in Pediatrics, 2019, 7, 43.	0.9	5
52	Fast and robust active neuron segmentation in two-photon calcium imaging using spatiotemporal deep learning. Proceedings of the National Academy of Sciences of the United States of America, 2019, 116, 8554-8563.	3.3	91
53	MimickNet, Matching Clinical Post-Processing Under Realistic Black-Box Constraints. , 2019, , .		3
54	In vivo measurement of trabecular meshwork stiffness in a corticosteroid-induced ocular hypertensive mouse model. Proceedings of the National Academy of Sciences of the United States of America, 2019, 116, 1714-1722.	3.3	66

#	Article	lF	CITATIONS
55	Effect of Ciliary Neurotrophic Factor on Retinal Neurodegeneration in Patients with Macular Telangiectasia Type 2. Ophthalmology, 2019, 126, 540-549.	2.5	110
56	RAC-CNN: multimodal deep learning based automatic detection and classification of rod and cone photoreceptors in adaptive optics scanning light ophthalmoscope images. Biomedical Optics Express, 2019, 10, 3815.	1.5	30
57	Hybrid light-sheet and light-field microscope for high resolution and large volume neuroimaging. Biomedical Optics Express, 2019, 10, 6595.	1.5	25
58	Reply. American Journal of Ophthalmology, 2018, 189, 178.	1.7	1
59	Comparison of chorioretinal layers in rhesus macaques using spectral-domain optical coherence tomography and high-resolution histological sections. Experimental Eye Research, 2018, 168, 69-76.	1.2	31
60	Linking OCT, Angiographic, and Photographic Lesion Components in Neovascular Age-Related Macular Degeneration. Ophthalmology Retina, 2018, 2, 481-493.	1.2	10
61	Novel Image-Based Analysis for Reduction of Clinician-Dependent Variability in Measurement of the Corneal Ulcer Size. Cornea, 2018, 37, 331-339.	0.9	23
62	Information-Theoretic Approach and Fundamental Limits of Resolving Two Closely Timed Neuronal Spikes in Mouse Brain Calcium Imaging. IEEE Transactions on Biomedical Engineering, 2018, 65, 2428-2439.	2.5	4
63	Choroidal Changes After Suprachoroidal Injection of Triamcinolone Acetonide in Eyes With Macular Edema Secondary to Retinal Vein Occlusion. American Journal of Ophthalmology, 2018, 186, 144-151.	1.7	42
64	Deep learning based detection of cone photoreceptors with multimodal adaptive optics scanning light ophthalmoscope images of achromatopsia. Biomedical Optics Express, 2018, 9, 3740.	1.5	41
65	Deep longitudinal transfer learning-based automatic segmentation of photoreceptor ellipsoid zone defects on optical coherence tomography images of macular telangiectasia type 2. Biomedical Optics Express, 2018, 9, 2681.	1.5	48
66	Real-time corneal segmentation and 3D needle tracking in intrasurgical OCT. Biomedical Optics Express, 2018, 9, 2716.	1.5	36
67	Statistical Models of Signal and Noise and Fundamental Limits of Segmentation Accuracy in Retinal Optical Coherence Tomography. IEEE Transactions on Medical Imaging, 2018, 37, 1978-1988.	5.4	36
68	Handheld adaptive optics scanning laser ophthalmoscope. Optica, 2018, 5, 1027.	4.8	26
69	Evaluation of inner retinal layers as biomarkers in mild cognitive impairment to moderate Alzheimer's disease. PLoS ONE, 2018, 13, e0192646.	1.1	88
70	Open-source, machine and deep learning-based automated algorithm for gestational age estimation through smartphone lens imaging. Biomedical Optics Express, 2018, 9, 6038.	1.5	8
71	Effects of aging and environmental tobacco smoke exposure on ocular and plasma circulatory microRNAs in the Rhesus macaque. Molecular Vision, 2018, 24, 633-646.	1.1	9
72	Anatomy and spatial organization of Müller glia in mouse retina. Journal of Comparative Neurology, 2017, 525, spc1-spc1.	0.9	1

#	Article	IF	CITATIONS
73	Anatomy and spatial organization of Müller glia in mouse retina. Journal of Comparative Neurology, 2017, 525, 1759-1777.	0.9	71
74	Macular Fluid Reduces Reproducibility of Choroidal Thickness Measurements on Enhanced Depth Optical Coherence Tomography. American Journal of Ophthalmology, 2017, 184, 108-114.	1.7	16
75	Open source software for automatic detection of cone photoreceptors in adaptive optics ophthalmoscopy using convolutional neural networks. Scientific Reports, 2017, 7, 6620.	1.6	65
76	In Vivo Multimodal Imaging of Drusenoid Lesions in Rhesus Macaques. Scientific Reports, 2017, 7, 15013.	1.6	38
77	Segmentation Based Sparse Reconstruction of Optical Coherence Tomography Images. IEEE Transactions on Medical Imaging, 2017, 36, 407-421.	5.4	107
78	Optical Coherence Tomography Predictors of Risk for Progression to Non-Neovascular Atrophic Age-Related Macular Degeneration. Ophthalmology, 2017, 124, 1764-1777.	2.5	77
79	Wide-field retinal optical coherence tomography with wavefront sensorless adaptive optics for enhanced imaging of targeted regions. Biomedical Optics Express, 2017, 8, 16.	1.5	40
80	Automatic segmentation of nine retinal layer boundaries in OCT images of non-exudative AMD patients using deep learning and graph search. Biomedical Optics Express, 2017, 8, 2732.	1.5	396
81	Retinal imaging in human autopsy eyes using a custom optical coherence tomography periscope. Biomedical Optics Express, 2017, 8, 4152.	1.5	4
82	Correlation Between Macular Integrity Assessment and Optical Coherence Tomography Imaging of Ellipsoid Zone in Macular Telangiectasia Type 2. , 2017, 58, BIO291.		29
83	A Quantitative Approach to Predict Differential Effects of Anti-VEGF Treatment on Diffuse and Focal Leakage in Patients with Diabetic Macular Edema: A Pilot Study. Translational Vision Science and Technology, 2017, 6, 7.	1.1	28
84	Platform-Independent Cirrus and Spectralis Thickness Measurements in Eyes with Diabetic Macular Edema Using Fully Automated Software. Translational Vision Science and Technology, 2017, 6, 9.	1.1	10
85	Enhanced visualization of peripheral retinal vasculature with wavefront sensorless adaptive optics optical coherence tomography angiography in diabetic patients. Optics Letters, 2017, 42, 17.	1.7	30
86	Characterization of Long Working Distance Optical Coherence Tomography for Imaging of Pediatric Retinal Pathology. Translational Vision Science and Technology, 2017, 6, 12.	1.1	7
87	Using an Image Fusion Methodology to Improve Efficiency and Traceability of Posterior Pole Vessel Analysis by ROPtool. Open Ophthalmology Journal, 2017, 11, 143-151.	0.1	2
88	The Effects of Diabetic Retinopathy and Pan-Retinal Photocoagulation on Photoreceptor Cell Function as Assessed by Dark Adaptometry. , 2016, 57, 208.		36
89	Impact of Microscope-Integrated OCT on Ophthalmology Resident Performance of Anterior Segment Surgical Maneuvers in Model Eyes. , 2016, 57, OCT146.		32
90	Posterior Eye Shape Measurement With Retinal OCT Compared to MRI. , 2016, 57, OCT196.		39

#	Article	IF	CITATIONS
91	Understanding RPE Lipofuscin. , 2016, 57, 6766.		3
92	Longitudinal Associations Between Microstructural Changes and Microperimetry in the Early Stages of Age-Related Macular Degeneration. , 2016, 57, 3714.		46
93	Effect of Uveal Melanocytes on Choroidal Morphology in Rhesus Macaques and Humans on Enhanced-Depth Imaging Optical Coherence Tomography. , 2016, 57, 5764.		40
94	Semiautomatic Segmentation of Rim Area Focal Hyperautofluorescence Predicts Progression of Geographic Atrophy Due to Dry Age-Related Macular Degeneration. , 2016, 57, 2283.		21
95	Analyzing spatial correlations in tissue using angle-resolved low coherence interferometry measurements guided by co-located optical coherence tomography. Biomedical Optics Express, 2016, 7, 1400.	1.5	14
96	Segmentation guided registration of wide field-of-view retinal optical coherence tomography volumes. Biomedical Optics Express, 2016, 7, 4827.	1.5	17
97	Repeatability of Choroidal Thickness Measurements on Enhanced Depth Imaging Optical Coherence Tomography Using Different Posterior Boundaries. American Journal of Ophthalmology, 2016, 169, 104-112.	1.7	43
98	Relating Retinal Morphology and Function in Aging and Early to Intermediate Age-related Macular Degeneration Subjects. American Journal of Ophthalmology, 2016, 165, 65-77.	1.7	43
99	Retinal nerve fiber layer thickness in amnestic mild cognitive impairment: Caseâ€control study and metaâ€analysis. Alzheimer's and Dementia: Diagnosis, Assessment and Disease Monitoring, 2016, 4, 85-93.	1.2	51
100	In vivo cellular-resolution retinal imaging in infants and children using an ultracompact handheld probe. Nature Photonics, 2016, 10, 580-584.	15.6	40
101	Automatic detection of cone photoreceptors in split detector adaptive optics scanning light ophthalmoscope images. Biomedical Optics Express, 2016, 7, 2036.	1.5	55
102	Length-adaptive graph search for automatic segmentation of pathological features in optical coherence tomography images. Journal of Biomedical Optics, 2016, 21, 076015.	1.4	31
103	Optical Coherence Tomography Reflective Drusen Substructures Predict Progression to Geographic Atrophy in Age-related Macular Degeneration. Ophthalmology, 2016, 123, 2554-2570.	2.5	69
104	Validation of Macular Choroidal Thickness Measurements from Automated SD-OCT Image Segmentation. Optometry and Vision Science, 2016, 93, 1387-1398.	0.6	17
105	Needle Depth and Big-Bubble Success in Deep Anterior Lamellar Keratoplasty. Cornea, 2016, 35, 1471-1477.	0.9	32
106	Macular sub-layer thinning and association with pulmonary function tests in Amyotrophic Lateral Sclerosis. Scientific Reports, 2016, 6, 29187.	1.6	32
107	Visualization of conventional outflow tissue responses to netarsudil in living mouse eyes. European Journal of Pharmacology, 2016, 787, 20-31.	1.7	89
108	Drusen Volume and Retinal Pigment Epithelium Abnormal Thinning Volume Predict 2-Year Progression of Age-Related Macular Degeneration. Ophthalmology, 2016, 123, 39-50.e1.	2.5	92

#	Article	IF	CITATIONS
109	Reply. Ophthalmology, 2016, 123, e6-e7.	2.5	0
110	INTRAOPERATIVE SPECTRAL DOMAIN OPTICAL COHERENCE TOMOGRAPHY IMAGING AFTER INTERNAL LIMITING MEMBRANE PEELING IN IDIOPATHIC EPIRETINAL MEMBRANE WITH CONNECTING STRANDS. Retina, 2015, 35, 1622-1630.	1.0	20
111	Intrasurgical Human Retinal Imaging With Manual Instrument Tracking Using a Microscope-Integrated Spectral-Domain Optical Coherence Tomography Device. Translational Vision Science and Technology, 2015, 4, 1.	1.1	33
112	Fully Automatic Segmentation of Fluorescein Leakage in Subjects With Diabetic Macular Edema. Investigative Ophthalmology and Visual Science, 2015, 56, 1482-1492.	3.3	68
113	Physical Factors Affecting Outflow Facility Measurements in Mice. , 2015, 56, 8331.		33
114	Retinal Atrophy in Eyes With Resolved Papilledema Detected by Optical Coherence Tomography. Journal of Neuro-Ophthalmology, 2015, 35, 122-126.	0.4	15
115	3-D Adaptive Sparsity Based Image Compression With Applications to Optical Coherence Tomography. IEEE Transactions on Medical Imaging, 2015, 34, 1306-1320.	5.4	26
116	Tree Topology Estimation. IEEE Transactions on Pattern Analysis and Machine Intelligence, 2015, 37, 1688-1701.	9.7	47
117	Multimodal Characterization of Proliferative Diabetic Retinopathy Reveals Alterations in Outer Retinal Function and Structure. Ophthalmology, 2015, 122, 957-967.	2.5	49
118	Assessment of Retinal Nerve Fiber Layer Thickness in Healthy, Full-Term Neonates. American Journal of Ophthalmology, 2015, 159, 803-811.e2.	1.7	26
119	Ultra-compact switchable SLO/OCT handheld probe design. , 2015, , .		0
120	Optical Coherence Tomography Accurately Measures Corneal Power Change from Laser Refractive Surgery. Ophthalmology, 2015, 122, 677-686.	2.5	39
121	Relationship of Central Choroidal Thickness With Age-Related Macular Degeneration Status. American Journal of Ophthalmology, 2015, 159, 617-626.e2.	1.7	77
122	Kernel regression based segmentation of optical coherence tomography images with diabetic macular edema. Biomedical Optics Express, 2015, 6, 1172.	1.5	265
123	Retinal Artery-Vein Classification via Topology Estimation. IEEE Transactions on Medical Imaging, 2015, 34, 2518-2534.	5.4	126
124	Pilocarpine-Induced Dilation of Schlemm's Canal and Prevention of Lumen Collapse at Elevated Intraocular Pressures in Living Mice Visualized by OCT. , 2014, 55, 3737.		74
125	Lateral and axial measurement differences between spectral-domain optical coherence tomography systems. Journal of Biomedical Optics, 2014, 19, 016014.	1.4	26
126	Compressed wavefront sensing. Optics Letters, 2014, 39, 1189.	1.7	13

#	Article	IF	CITATIONS
127	Automatic segmentation of up to ten layer boundaries in SD-OCT images of the mouse retina with and without missing layers due to pathology. Biomedical Optics Express, 2014, 5, 348.	1.5	104
128	True color scanning laser ophthalmoscopy and optical coherence tomography handheld probe. Biomedical Optics Express, 2014, 5, 3204.	1.5	27
129	Fully automated detection of diabetic macular edema and dry age-related macular degeneration from optical coherence tomography images. Biomedical Optics Express, 2014, 5, 3568.	1.5	362
130	Characterization of the Choroid-Scleral Junction and Suprachoroidal Layer in Healthy Individuals on Enhanced-Depth Imaging Optical Coherence Tomography. JAMA Ophthalmology, 2014, 132, 174.	1.4	93
131	Effect of Anti–Vascular Endothelial Growth Factor Therapy on Choroidal Thickness in Diabetic Macular Edema. American Journal of Ophthalmology, 2014, 158, 745-751.e2.	1.7	87
132	Coherence revival multiplexed, buffered swept source optical coherence tomography: 400  kHz imaging with a 100  kHz source. Optics Letters, 2014, 39, 3740.	1.7	19
133	Quantitative Classification of Eyes with and without Intermediate Age-related Macular Degeneration Using Optical Coherence Tomography. Ophthalmology, 2014, 121, 162-172.	2.5	280
134	Disease progression in iridocorneal angle tissues of BMP2-induced ocular hypertensive mice with optical coherence tomography. Molecular Vision, 2014, 20, 1695-709.	1.1	18
135	Correction of Ocular Shape in Retinal Optical Coherence Tomography and Effect on Current Clinical Measures. American Journal of Ophthalmology, 2013, 156, 304-311.	1.7	58
136	Progression of Intermediate Age-related Macular Degeneration with Proliferation and Inner Retinal Migration of Hyperreflective Foci. Ophthalmology, 2013, 120, 1038-1045.	2.5	208
137	Fast Acquisition and Reconstruction of Optical Coherence Tomography Images via Sparse Representation. IEEE Transactions on Medical Imaging, 2013, 32, 2034-2049.	5.4	191
138	Automated non-rigid registration and mosaicing for robust imaging of distinct retinal capillary beds using speckle variance optical coherence tomography. Biomedical Optics Express, 2013, 4, 803.	1.5	139
139	Automatic cone photoreceptor segmentation using graph theory and dynamic programming. Biomedical Optics Express, 2013, 4, 924.	1.5	75
140	Handheld simultaneous scanning laser ophthalmoscopy and optical coherence tomography system. Biomedical Optics Express, 2013, 4, 2307.	1.5	66
141	Optimization of confocal scanning laser ophthalmoscope design. Journal of Biomedical Optics, 2013, 18, 076015.	1.4	31
142	Fully Automatic Software for Retinal Thickness in Eyes With Diabetic Macular Edema From Images Acquired by Cirrus and Spectralis Systems. , 2013, 54, 7595.		58
143	Choroid Development and Feasibility of Choroidal Imaging in the Preterm and Term Infants Utilizing SD-OCT. , 2013, 54, 4140.		69
144	Visualization of Real-Time Intraoperative Maneuvers with a Microscope-Mounted Spectral Domain Optical Coherence Tomography System. Retina, 2013, 33, 232-236.	1.0	83

#	Article	IF	CITATIONS
145	Dry Age-Related Macular Degeneration: Mechanisms, Therapeutic Targets, and Imaging. , 2013, 54, ORSF68.		218
146	Macular Findings in Healthy Full-term Hispanic Newborns Observed by Hand-held Spectral-Domain Optical Coherence Tomography. Ophthalmic Surgery Lasers and Imaging Retina, 2013, 44, 448-454.	0.4	15
147	Image Inversion Spectral-Domain Optical Coherence Tomography Optimizes Choroidal Thickness and Detail through Improved Contrast. , 2012, 53, 1874.		28
148	Exploratory Dijkstra forest based automatic vessel segmentation: applications in video indirect ophthalmoscopy (VIO). Biomedical Optics Express, 2012, 3, 327.	1.5	37
149	Sparsity based denoising of spectral domain optical coherence tomography images. Biomedical Optics Express, 2012, 3, 927.	1.5	225
150	Automatic segmentation of closed-contour features in ophthalmic images using graph theory and dynamic programming. Biomedical Optics Express, 2012, 3, 1127.	1.5	65
151	Corneal biometry from volumetric SDOCT and comparison with existing clinical modalities. Biomedical Optics Express, 2012, 3, 1279.	1.5	15
152	Distributed scanning volumetric SDOCT for motion corrected corneal biometry. Biomedical Optics Express, 2012, 3, 2050.	1.5	25
153	Spectral-Domain Optical Coherence Tomographic Assessment of Severity of Cystoid Macular Edema in Retinopathy of Prematurity. JAMA Ophthalmology, 2012, 130, 569-78.	2.6	98
154	Validated Automatic Segmentation of AMD Pathology Including Drusen and Geographic Atrophy in SD-OCT Images. , 2012, 53, 53.		204
155	Foveal avascular zone and foveal pit formation after preterm birth. British Journal of Ophthalmology, 2012, 96, 961-966.	2.1	110
156	Subfoveal Fluid in Healthy Full-term Newborns Observed by Handheld Spectral-Domain Optical Coherence Tomography. American Journal of Ophthalmology, 2012, 153, 167-175.e3.	1.7	42
157	Maturation of the Human Fovea: Correlation of Spectral-Domain Optical Coherence Tomography Findings With Histology. American Journal of Ophthalmology, 2012, 154, 779-789.e2.	1.7	193
158	Distributed Scan SDOCT Improves Post Refractive Surgery Corneal Biometry. , 2012, , .		0
159	Spatial Correlation between Hyperpigmentary Changes on Color Fundus Photography and Hyperreflective Foci on SDOCT in Intermediate AMD. , 2012, 53, 4626.		80
160	Robust automatic segmentation of corneal layer boundaries in SDOCT images using graph theory and dynamic programming. Biomedical Optics Express, 2011, 2, 1524.	1.5	101
161	Enhanced video indirect ophthalmoscopy (VIO) via robust mosaicing. Biomedical Optics Express, 2011, 2, 2871.	1.5	31
162	Dynamics of Human Foveal Development after Premature Birth. Ophthalmology, 2011, 118, 2315-2325.	2.5	189

#	Article	IF	CITATIONS
163	Integration of a Spectral Domain Optical Coherence Tomography System into a Surgical Microscope for Intraoperative Imaging. , 2011, 52, 3153.		165
164	Analysis of Pars Plana Vitrectomy for Optic Pit–Related Maculopathy With Intraoperative Optical Coherence Tomography. JAMA Ophthalmology, 2011, 129, 1483.	2.6	73
165	Proteomic Profiling of a Layered Tissue Reveals Unique Glycolytic Specializations of Photoreceptor Cells. Molecular and Cellular Proteomics, 2011, 10, M110.002469.	2.5	72
166	Anti-amyloid therapy protects against retinal pigmented epithelium damage and vision loss in a model of age-related macular degeneration. Proceedings of the National Academy of Sciences of the United States of America, 2011, 108, E279-87.	3.3	185
167	Quantitative Comparison of Drusen Segmented on SD-OCT versus Drusen Delineated on Color Fundus Photographs. , 2010, 51, 4875.		99
168	Evaluation of Contrast Agents for Enhanced Visualization in Optical Coherence Tomography. , 2010, 51, 6614.		30
169	Segmentation of ophthalmic optical coherence tomography images using graph cuts. , 2010, , .		0
170	Interlaced spectrally encoded confocal scanning laser ophthalmoscopy and spectral domain optical coherence tomography. Biomedical Optics Express, 2010, 1, 431.	1.5	30
171	Automatic segmentation of seven retinal layers in SDOCT images congruent with expert manual segmentation. Optics Express, 2010, 18, 19413.	1.7	639
172	Efficient Fourier-Wavelet Super-Resolution. IEEE Transactions on Image Processing, 2010, 19, 2669-2681.	6.0	76
173	Abnormal Foveal Morphology in Ocular Albinism Imaged With Spectral-Domain Optical Coherence Tomography. JAMA Ophthalmology, 2009, 127, 37.	2.6	124
174	Photoreceptor Layer Thinning over Drusen in Eyes with Age-Related Macular Degeneration Imaged In Vivo with Spectral-Domain Optical Coherence Tomography. Ophthalmology, 2009, 116, 488-496.e2.	2.5	251
175	Insights into Advanced Retinopathy of Prematurity Using Handheld Spectral Domain Optical Coherence Tomography Imaging. Ophthalmology, 2009, 116, 2448-2456.	2.5	165
176	Imaging the Infant Retina with a Hand-held Spectral-Domain Optical Coherence Tomography Device. American Journal of Ophthalmology, 2009, 147, 364-373.e2.	1.7	164
177	Power Trace: An Efficient Method for Extracting the Power Dissipation Profile in an IC Chip From Its Temperature Map. IEEE Transactions on Components and Packaging Technologies, 2009, 32, 309-316.	1.4	13
178	Generalized pseudo-polar Fourier grids and applications in registering ophthalmic optical coherence tomography images. , 2009, , .		4
179	INTRAOPERATIVE USE OF HANDHELD SPECTRAL DOMAIN OPTICAL COHERENCE TOMOGRAPHY IMAGING IN MACULAR SURGERY. Retina, 2009, 29, 1457-1468.	1.0	165
180	Applications of Spectral-Domain OCT in AMD. , 2009, , 15-34.		1

#	Article	IF	CITATIONS
181	Deblurring Using Regularized Locally Adaptive Kernel Regression. IEEE Transactions on Image Processing, 2008, 17, 550-563.	6.0	143
182	Efficient restoration and enhancement of super-resolved X-ray images. , 2008, , .		4
183	Fast detection and segmentation of drusen in retinal optical coherence tomography images. Proceedings of SPIE, 2008, , .	0.8	27
184	Efficient Registration of Aliased X-Ray Images. Conference Record of the Asilomar Conference on Signals, Systems and Computers, 2007, , .	0.0	7
185	Higher order bilateral filters and their properties. , 2007, , .		11
186	Multi-Scale Statistical Detection and Ballistic Imaging Through Turbid Media. , 2007, , .		0
187	Statistical detection and imaging of objects hidden in turbid media using ballistic photons. Applied Optics, 2007, 46, 5805.	2.1	27
188	Extraction of Power Dissipation Profile in an IC Chip from Temperature Map. IEEE Semiconductor Thermal Measurement and Management Symposium, 2007, , .	0.0	5
189	Kernel Regression for Image Processing and Reconstruction. IEEE Transactions on Image Processing, 2007, 16, 349-366.	6.0	1,114
190	Multiframe demosaicing and super-resolution of color images. IEEE Transactions on Image Processing, 2006, 15, 141-159.	6.0	262
191	Video-to-Video Dynamic Super-Resolution for Grayscale and Color Sequences. Eurasip Journal on Advances in Signal Processing, 2006, 2006, 1.	1.0	39
192	A practical approach to superresolution. , 2006, 6077, 24.		9
193	Regularized Kernel Regression for Image Deblurring. , 2006, , .		2
194	Robust Kernel Regression for Restoration and Reconstruction of Images from Sparse Noisy Data. , 2006, , .		33
195	<title>Dynamic demosaicing and color superresolution of video sequences</title> ., 2004, , .		13
196	Advances and challenges in super-resolution. International Journal of Imaging Systems and Technology, 2004, 14, 47-57.	2.7	526
197	Fast and Robust Multiframe Super Resolution. IEEE Transactions on Image Processing, 2004, 13, 1327-1344.	6.0	1,689
198	Multiframe demosaicing and super-resolution from undersampled color images. , 2004, 5299, 222.		19

12

#	Article	IF	CITATIONS
199	Robust shift and add approach to superresolution. , 2003, , .		50
200	Prediction of lupus nephritis in patients with systemic lupus erythematosus using artificial neural networks. Lupus, 2002, 11, 485-492.	0.8	13
201	Novel approaches to high-speed multi-view imaging approaching 4pi steradians using conic section mirrors: theoretical and practical considerations. Journal of the Optical Society of America A: Optics and Image Science, and Vision, 0, , .	0.8	3
202	Computational 3D microscopy with optical coherence refraction tomography. Optica, 0, , .	4.8	8